Arch. Met. Geoph. Biokl., Ser. A, 27, 1–19 (1978)

ARCHIV
FÜR METEOROLOGIE
GEOPHYSIK UND
BIOKLIMATOLOGIE

551.509.313

National Research Institute for Mathematical Sciences, CSIR, Pretoria, South Africa;
The Israeli Meteorological Service, Beth-Dagan, Israel

Application of Fourth-Order Finite Differences to a Baroclinic Model of the Atmosphere

I. M. Navon and **Z. Alperson**

With 7 Figures

Received June 3, 1977

Summary

Fourth-order difference approximations are implemented in a three-parameter baroclinic quasigeostrophic model of the atmosphere based on a modified version of the Bushby-Whitelam [2] model, currently in use at the Israeli Meteorological Office.
The fourth-order accurate numerical forecast on a mesh covering Europe and the Mediterranean regions results in improved locations of low- and high-pressure centres as compared with the second-order forecast. The scheme also yields better estimates of the changes in position and intensity of the synoptic systems. The fourth-order numerical forecast tends, however, to lower the values at the pressure centres. This so-called pillow effect still has to be explained.

Zusammenfassung

Anwendung des Differenzenverfahrens vierter Ordnung auf ein baroklines Modell der Atmosphäre

Differenzenverfahren vierter Ordnung werden auf ein drei-Parameter baroklines quasigeostrophes Modell der Atmosphäre angewendet. Dieses Atmosphärenmodell, welches zur Zeit am israelischen meteorologischen Büro benutzt wird, ist eine Modifikation des Bushby-Whitelam Modells [2].
Die numerische Vorhersage vierter Ordnung, die sich über Europa und das Mittelmeer erstreckt, ergibt eine bessere Lokalisierung der Hoch- und Tiefdruckzentren, als dies mit einer Vorhersage zweiter Ordnung möglich wäre. Sie führt auch zu besseren Abschätzungen der Positions- und Intensitätsänderungen des synoptischen Systems. Anderseits aber strebt sie dazu, die Werte in den Druckzentren zu verringern. Dieser sogenannte „pillow effect" muß noch weiter untersucht werden.

0066-6416/78/0027/0001/$ 03.80

1. Introduction

The computational advantage of fourth-order accurate finite difference approximations over those of second-order in reducing truncation and phase errors has been established by several investigators (e. g. [7, 10, 12, 14, 16]). Kreiss and Oliger [8, 9] established that fourth-order accurate methods are optimal in the sense that the gain in accuracy obtained by using difference approximations of order higher than four is minimal in view of the volume of computational work involved. On the other hand, as remarked by Grammeltvedt [4], fourth-order differencing schemes increase the magnitude of the interaction coefficients for the aliasing terms. Partially to overcome this disadvantage a selective dissipative term suggested by Kreiss and Oliger [9] is introduced here; this renders the approximation dissipative and makes it possible to control the amount of dissipation.
In Section 2 the main features of the atmospheric model are described, including its basic prognostic equations. The fourth-order accurate finite difference expressions for the differential operators used in the model equations, e. g. the fourth-order Jacobians and Laplacians, are derived in Section 3. The dissipative term is introduced in Section 4 and it is shown that this term renders a fourth-order scheme (using leap-frog time differencing) dissipative and stable. Some numerical aspects of the introduction of the fourth-order differences are discussed in Section 5.
Finally, the results of operative numerical forecasts using fourth-order finite differences are presented in Section 6. Statistical results are presented for two sequences of 24-hour forecasts, while a particular sequence of forecasts is synoptically discussed and illustrated by figures.

2. The Three-Parameter Baroclinic Model

2.1 Main Features of the Atmospheric Model

The three-parameter model used in the numerical experiments is a modified version of the Bushby-Whitelam [2] model currently in operative use at the Israeli Meteorological Service. The model consists of two layers of shearing fluid bounded respectively by the pressure surface p_0 = 1000 mb, p_m = 600 mb and p_1 = 200 mb. Within each layer the thermal wind is taken to be constant in direction and assumed to have a speed varying linearly with pressure through the layer.
The winds are obtained from the geostrophic relationship. Pressure is used as a vertical coordinate and the hydrostatic approximation is used in deriving the equations of motion; in this way sound waves are eliminated from the solution [17]. The vertical velocity is assumed to vary parabolically with pressure in each of the two layers, vanishing at the upper boundary

surface, and it is determined at the lower boundary by the effects of forced vertical motion over the topography, and by surface friction. The vertical velocity at the interface $p_m = 600$ mb is continuous.
The only non-adiabatic heating effect taken into account is that of a warm sea heating cold air above it: this effect is confined to the lower layer. The twisting term and the vertical advection of vorticity are neglected. The topography is approximated by taking at each grid point a height equal to the mean height over a symmetrical surrounding square of side one grid length. Surface equations of horizontal motion involve a constant coefficient of turbulence, a procedure which gives the Ekman spiral variation of wind with height in the friction layer. The surface wind is supposed to blow over land into low-pressure areas at an angle of 30° to the 1000 mb contour, to have a speed 0,35 times that of the corresponding geostrophic wind, and to blow over sea at a 3° angle and at a speed 0,85 times that of the geostrophic wind.

2.2 Basic Equations

List of symbols used

f	Coriolis parameter
g	acceleration due to gravity
p	atmospheric pressure
p_0	1000 mb pressure
p_m	600 mb pressure
p_1	200 mb pressure
h_0'	1000/600 mb layer thickness
h_1'	600/200 mb layer thickness
Q_0	rate of heating of lower layer of air over a warmer sea
R	gas constant of air
t	time
V_0'	thermal wind in the lower layer
V_1'	thermal wind in the upper layer
β	map magnification factor from earth to plane = $1.866/(1 + \sin\phi)$
Γ_0	lapse rate in the lower layer = -0.0422222°C/mb
Γ_1	lapse rate in the upper layer = -0.051111°C/mb
ϕ	latitude
ψ	stream function
$\omega = \frac{dp}{dt}$	vertical velocity
ω_0	vertical velocity at 1000 mb
∇^2	Laplacian operator
$J(A, b)$	Jacobian operator

Five partial differential equations have to be solved for five unknowns, viz. the time rates of change of the thicknesses h_0', h_1' in the two layers, the time

rate of change of the stream function ψ, and two coefficients in the vertical velocity formulae.
The equations (after [2]) are as follows.

$$\nabla^2\left(\frac{\partial\psi}{\partial t}\right)+J(\psi,\beta^2\nabla^2\psi+f)+\frac{g}{12f}J\left(\beta^2\frac{g}{f}\nabla^2h_0',h_0'\right)+\frac{g}{12f}J(\beta^2\frac{g}{f}\nabla^2h_1',h_1')=$$
$$=\frac{1}{2(p_0-p_1)}\left\{-4b\left(\nabla^2\psi+\frac{f}{\beta^2}\right)+\frac{ag}{f}(\nabla^2h_0'+\nabla^2h_1')-\frac{bg}{f}(\nabla^2h_1'-\nabla^2h_0')\right\}+$$
$$+\frac{\omega_0}{(p_0-p_1)}\left\{\frac{g}{8f}(\nabla^2h_0'+\nabla^2h_1')+\frac{f}{\beta^2}\right\}. \tag{1}$$

$$\nabla^2\left(\frac{\partial h_0'}{\partial t}\right)+\frac{f}{g}J\left(\psi,\frac{\beta^2g}{f}\nabla^2h_0'\right)+J\left(h_0',\beta^2\nabla^2\psi+f-\frac{\beta^2g}{f}\nabla^2h_0'\right)=$$
$$=-\frac{2}{(p_0-p_1)}\left(a+\frac{\omega_0}{4}+b\right)\left(2\left(\frac{f}{g}\nabla^2\psi+\frac{f^2}{g\beta^2}\right)-\nabla^2h_0'\right). \tag{2}$$

$$\nabla^2\left(\frac{\partial h_1'}{\partial t}\right)+\frac{f}{g}J\left(\psi,\beta^2\frac{g}{f}\nabla^2h_1'\right)+J\left(h_1',\beta^2\nabla^2\psi+f+\frac{\beta^2g}{f}\nabla^2h_1'\right)=$$
$$=-\frac{2}{(p_0-p_1)}\left(a+\frac{\omega_0}{4}-b\right)\left(2\left(\frac{f}{g}\nabla^2\psi+\frac{f^2}{g\beta^2}\right)+\nabla^2h_1'\right). \tag{3}$$

$$\frac{\partial h_0'}{\partial t}=-H+A\left(a+\frac{\omega_0}{4}\right)+Bb \tag{4}$$

where $H=\beta^2J(\psi,h_0')-Q_0-\left(E'-\frac{A}{4}\right)\omega_0$

$a=0.125\,(p_0-p_1)\,(\text{div}\,V_0'+\text{div}\,V_1')-0.25\,\omega_0$

$b=0.125\,(p_0-p_1)\,(\text{div}\,V_0'-\text{div}\,V_1')$

$$\frac{\partial h_1'}{\partial t}=-I+C\left(a+\frac{\omega_0}{4}\right)+Db \tag{5}$$

where $I=\beta^2J(\psi,h_1')-\left(F'-\frac{C}{4}\right)\omega_0.$

Solving (4) and (5) for $a+\frac{\omega_0}{4}$ and b we have

$$a+\frac{\omega_0}{4}=\frac{D}{AD-BC}\left(H+\frac{\partial h_0'}{\partial t}\right)-\frac{B}{AD-BC}\left(I+\frac{\partial h_1'}{\partial t}\right) \tag{6}$$

$$b=-\frac{C}{AD-BC}\left(H+\frac{\partial h_0'}{\partial t}\right)+\frac{A}{AD-BC}\left(I+\frac{\partial h_1'}{\partial t}\right): \tag{7}$$

Substituting $a + \frac{\omega_0}{4}$ and b from (6) and (7) into (2) and (3), we obtain two simultaneous partial differential equations of Helmholtz type for $\frac{\partial h_0'}{\partial t}$ and $\frac{\partial h_1'}{\partial t}$:

$$\nabla^2\left(\frac{\partial h_0'}{\partial t}\right) + E\left(\frac{\partial h_0'}{\partial t}\right) + F\left(\frac{\partial h_1'}{\partial t}\right) + G = 0 \tag{8}$$

$$\nabla^2\left(\frac{\partial h_1'}{\partial t}\right) + L\left(\frac{\partial h_0'}{\partial t}\right) + M\left(\frac{\partial h_1'}{\partial t}\right) + N = 0. \tag{9}$$

The symbols E, F, G, L. M, N are defined in the appendix.
The 600 mb height h_m is obtained from the stream function by solving the balance equation

$$\nabla^2\psi = \frac{g}{f}\nabla^2 h_m - \frac{2}{f}\left(\frac{\partial^2\psi}{\partial x^2}\frac{\partial^2\psi}{\partial y^2} - \left(\frac{\partial^2\psi}{\partial x \partial y}\right)^2\right) - \frac{\nabla f \cdot \nabla\psi}{f} \tag{10}$$

"in reverse".
The linear eqs. (1), (8) and (9) are discretized by finite difference approximations and the resulting algebraic equations are solved by iterative techniques. (S.O.R.)

2.3 Grid Mesh, Boundary Conditions, Computations

The Northern Hemisphere is mapped onto a polar stereographic projection true at 60°N for which the map factor is given by $\beta = 1.866/(1 + \sin\phi)$. The area under consideration is a rectangle inside the stereographic projection extending from latitude 10°N to 90° N and longitude 100°W to 95°E. The area is covered by a 48 × 29 horizontal grid system which gives a grid size of $\Delta x = \Delta y = 381$ km at 60°N.
For upper and lower boundary conditions the vertical velocity ω was taken to be zero at 200 mb pressure surface while it was taken to be equal to ω_0 at the 1000 mb pressure surface (at all grid points). Lateral boundary conditions were that there is no change in the heights of isobaric surfaces on the boundary during the period of the forecast.
The equation for the rate of change of the stream function (1) is a Poisson elliptic equation, while eqs. (8) and (9) for the rate of change of the thickness in the two layers are a pair of simultaneous Helmholtz equations. The equations are discretized by finite difference approximations and the resulting algebraic linear equations are solved by the successive overrelaxation (S.O.R.) iterative technique. A leap-frog time differencing scheme is employed throughout the numerical integration. To avoid separation of the odd and even time-step solutions, the odd and even solutions are averaged after a prescribed number of time-steps. A time-step of $\Delta t = 45$ minutes was used for the fourth-order model.

3. Fourth-Order Horizontal Finite-Difference Operators

We first define some basic difference operators to be used in this Section. We use the notation

$$u_{i,j}^n = u(i\,\Delta x, j\,\Delta y, n\,\Delta t), \qquad \begin{matrix} i = 1, 2, \ldots, N_x \\ j = 1, 2, \ldots, N_y \end{matrix} \tag{11}$$

where $N_x \Delta x = L$, $N_y \Delta y = D$. L and D being the horizontal dimensions of our rectangular domain. We now define

$$\begin{aligned} D_{+x} u_{i,j}^n &= (u_{i+1,j}^n - u_{i,j}^n)/\Delta x \\ D_{-x} u_{i,j}^n &= (u_{i,j}^n - u_{i-1,j}^n)/\Delta x \\ D_{ox} u_{i,j}^n &= (u_{i+1,j}^n - u_{i-1,j}^n)/2\,\Delta x. \end{aligned} \tag{12}$$

Similar definitions apply to D_{+y}, D_{-y}, D_{oy}.
Then a fourth-order finite-difference approximation to the first- and second-order derivatives of a function $u = u(x, y, t)$ in the x direction is

$$\left(\frac{\partial u}{\partial x}\right)_{i,j}^n = [(4/3)D_o(\Delta x) - (1/3)D_o(2\,\Delta x)]\, u_{i,j}^n + 0(\Delta x^4) \quad \text{or}$$

$$\left(\frac{\partial u}{\partial x}\right)_{i,j}^n = (u_{i-2,j} - 8\,u_{u-1,j} + 8\,u_{i+1,j} - u_{i-2,j})/12\,\Delta x + 0(\Delta x^4) \tag{13}$$

where $$D_o(n\,\Delta x)\, u_{i,j}^n = (2\,n\,\Delta x)^{-1}\,[u_{i+n,j}^n - u_{i-n,j}^n]. \tag{14}$$

For the second derivative we obtain

$$\left(\frac{\partial^2 u}{\partial x^2}\right)_{i,j}^n = [(4/3)\,D_o^2\left(\frac{\Delta x}{2}\right) - (1/3)\,D_o^2(\Delta x)]\, u_{i,j}^n + 0(\Delta x^4) \quad \text{or}$$

$$\left(\frac{\partial^2 u}{\partial x^2}\right)_{i,j}^n = (-u_{i-2,j}^n + 16\,u_{i-1,j}^n - 30\,u_{i,j}^n + 16\,u_{i+1,j}^n - u_{i+2,j}^n)/12\,\Delta x^2 + 0(\Delta x^4). \tag{15}$$

Similar expressions are obtained for the derivatives of u in the y direction. Assuming $\Delta x = \Delta y = h$, the fourth-order finite-difference expression for the Laplacian is

$$\begin{aligned} \nabla^2 u_{i,j}^n = \{&-60\,u_{i,j}^n + 16\,(u_{i+1,j}^n + u_{i-1,j}^n + u_{i,j+1}^n + u_{i,j-1}^n) - \\ &-(u_{i+2,j} + u_{i-2,j} + u_{i,j+2} + u_{i,j-2})\}/12\,h^2 + 0(h^4). \end{aligned} \tag{16}$$

We shall use the Arakawa [1] formulation for finite-difference Jacobians to obtain a fourth-order finite-difference approximation to the Jacobian $J(\zeta, \psi)$ of two functions $\zeta(x, y, t)$ and $\psi(x, y, t)$.
In his notation the fourth-order accurate Jacobian is

$$J(\zeta, \psi) = 2\,J_1(\alpha, \psi) - J_2(\zeta, \psi) + 0(h^4) \tag{17}$$

where J_1 and J_2 are two finite-difference analogues for the Jacobian

$$J_1(\zeta, \psi) = [J^{++}(\zeta, \psi) + J^{+x}(\zeta, \psi) + J^{x+}(\zeta, \psi)]/3, \tag{18}$$

$$J_2(\zeta, \psi) = [J^{xx}(\zeta, \psi) + J^{+x2}(\zeta, \psi) + J^{x+2}(\zeta, \psi)]/3, \tag{19}$$

the additional superscript 2 indicating that additional grid points $(i+2, j)$, $(i-2, j)$, $(i, j+2)$, $(i, j-2)$ are used. The finite-difference expressions for J^{++}, J^{+x}, J^{x+}, J^{xx}, J^{+x2} and J^{x+2} are given in [1].

Sundström [15] suggested a general method of constructing a fourth-order Jacobian from one of second order by

$$J(*)\,(f, g)_{i,j} = (4/3)\,J(h)\,(f, g)_{i,j} - (1/3)\,J(2h)\,(f, g)_{i,j} + 0(h^4), \tag{20}$$

where the * stands for 5- or 9-point second-order formulae for the Jacobian and $J(2h)$ means that we employ a double-space increment throughout. For instance, the 9-point Jacobian is

$$\begin{aligned} J(9)\,(f, g)_{i,j} = \frac{1}{4h}\Big\{ & \frac{a}{3}\,[(f_{i+1,j} - f_{i-1,j})\,(g_{i,j+1} - g_{i,j-1}) - \\ & - (f_{i,j+1} - f_{i,j-2})\,(g_{i+1,j} - g_{i-1,j})] + \frac{2-a}{3}\,[f_{i+1,j}(g_{i+1,j+1} - g_{i+1,j-1}) - \\ & - f_{i-1,j}(g_{i-1,j+1} - g_{i-1,j-1}) - f_{i,j+1}(g_{i+1,j+1} - g_{i-1,j+1}) + \\ & + f_{i,j-1}(g_{i+1,j-1} - g_{i-1,j-1})] + \frac{2-a}{3}\,[g_{i,j+2}(f_{i+1,j+1} - f_{i-1,j+1}) - \\ & - g_{i,j-1}(f_{i+1,j-1} - f_{i-1,j-1}) - g_{i+1,j}(f_{i+1,j+1} - f_{i+1,j-1}) + \\ & + g_{i-1,j}(f_{i-1,j+1} - f_{i-1,j-1})] + \frac{a-1}{3}\,\frac{1}{2}\,[(f_{i+1,j+1} - f_{i-1,j-1}) \cdot (g_{i-1,j+1} - g_{i+1,j-1}) - \\ & - (g_{i-1,j+1} - f_{i+1,j-1})\,(g_{i+1,j-1} - g_{i-1,j-1})]\Big\}\,. \end{aligned} \tag{21}$$

Using (20) and (21) with $a = 1$ we obtain the fourth-order Arakawa Jacobian. Sundström [15] suggests that it is better to take $a = 0$ to get the smallest phase-speed error. In our fourth-order model we used the Arakawa fourth-order Jacobian.

4. Inclusion of the Dissipative Term

Difficulties are experienced in the convergence of the iterative S.O.R. algorithm to the solution (within a prescribed accuracy) when fourth-order accurate space finite differences are employed. This effect is attributed to aliasing, due to the fact that the fourth-order scheme introduces larger aliasing coefficients than a second-order scheme. It was conjectured that if the short-wavelength components (which are the principal contributors to

aliasing) were removed, this difficulty would be overcome. Hence we included in our scheme a dissipative factor of the form suggested by Kreiss and Oliger [9], viz.

$$\frac{\epsilon h^6 D_+^3 D_-^3}{64}. \tag{22}$$

Including this term in the discretized solution of the simple hyperbolic system

$$\frac{\partial u}{\partial t} = A \frac{\partial u}{\partial x} \tag{23}$$

where A is a constant symmetric matrix, and using the leap-frog time discretization, we have

$$u_{i,j}^{n+1} = \left(I - \frac{\epsilon h^6 D_+^3 D_-^3}{64}\right) u_{i,j}^{n-1} + 2\Delta t A\,[(4/3) D_o(h) - (1/3) D_o(2h)]\, u_{i,j}^n. \tag{24}$$

This approximation is accurate of order $(\Delta t^2, \Delta x^4)$ but dissipative of order 6, as the eigenvalues of the amplification matrix are given by

$$|k_j| = 1 - \epsilon \sin^6 \frac{wh}{2} \quad \text{for} \quad |\lambda| = \left|\frac{\Delta t}{\Delta x}\right| < 1 - \epsilon, \quad \epsilon < 1 \tag{25}$$

$j = 1, 2, \ldots, n$ where n is the order of the matrix A and w is the frequency. The discretized form of the dissipative factor of order 6 in the x direction is

$$\left[\frac{\epsilon h^6}{64} D_{+x}^3 D_{-x}^3\right] u_{i,j}^n = \frac{\epsilon}{64} [u_{i+3,j}^n - 6 u_{i+2,j}^n + 15 u_{i+1,j}^n - 20 u_{i,j}^n + 15 u_{i-1,j}^n - 6 u_{i-2,j}^n + u_{i-3,j}^n], \tag{26}$$

and similarly in the y direction. A value of $\epsilon = 0.015$ was adopted for the calculations in our model.

At points adjacent to the boundaries a lower order of dissipativity was employed, viz. a term of the form

$$\frac{\epsilon h^4 D_+^2 D_-^2}{16}. \tag{27}$$

5. Numerical Aspects of the Fourth-Order Scheme and Baroclinic Model

5.1 The Time Step in the Fourth-Order Scheme

As pointed out by Gerrity et al. [3] the linear stability criterion has to be modified when higher-order difference approximations are used for the spatial derivatives.

If by $(\Delta t)_2$ we denote the limit on the time-step associated with the second-order scheme and by $(\Delta t)_4$ the corresponding limit for the fourth-order scheme, we obtain

$$(\Delta t)_4 \simeq 0.72\,(\Delta t)_2\,. \tag{28}$$

The use of the fourth-order scheme thus requires a 28 per cent reduction in the time-step used in the numerical integration.

5.2 Treatment of the Helmholtz Equations

In the three-parameter baroclinic model we have to solve a system of two simultaneous Helmholtz equations of the general form

$$\nabla^2\phi - \alpha(x,y)\phi = f(x,y), \tag{29}$$

where ∇^2, already defined, is the two dimensional Laplace operator, $\alpha(x, y)$ is non-negative and $f(x, y)$ is a "forcing function".
When approximated by a finite-difference scheme, eq. (29) reduces to a system of linear algebraic equations

$$Ax = b. \tag{30}$$

The size and the sign of the Helmholtz coefficient $\alpha(x, y)$ are extremely important as they determine whether or not the matrix A will be diagonally dominant, i. e. whether or not an iterative procedure for the solution of (30) will converge. To see this we take a finite-difference approximation to (29) using the fourth-order finite-difference Laplace operator (16) to get

$$\begin{aligned}(4/3)(u_{i+1,j} + u_{i-1,j} + u_{i,j+1} + u_{i,j-1}) - \\ -(1/12)(u_{i+2,j} + u_{i-2,j} + u_{i,j+2} + u_{i,j-2}) - (5 + \alpha h^2) = f(x, y)h^2\,.\end{aligned} \tag{31}$$

If in (31) $\alpha < 0$ we lose the diagonal dominance of the matrix A and are not assured of the convergence of an iterative method of solution for (30).
We can fall back on the discrete spectrum of the operator A and thus have a singular problem (Prof. G. Fairweather – personal communication). On the other hand for large values of $\alpha > 0$ the matrix A is strongly diagonally dominant and only few iterations are required when using for instance the S.O.R. iterative method.
By large α we mean here $h^2\alpha \gg 5$ and by small α, $h^2\alpha \ll 5$. In order that the systems of two simultaneous Helmholtz equations in our model should be diagonally dominant, the signs of the coefficients E and M in (8) and (9) should always be

$$E \leqslant 0;\quad M \leqslant 0. \tag{32}$$

Whenever E or M are violating the criteria given by (32) they are set to be 0. The minimal value of the Helmholtz coefficients in the integration domain is used to determine μ_B, the optimum relaxation factor for the S.O.R. method.

5.3 Boundary Conditions

Problems arise at points adjacent to the boundaries when the fourth-order accurate space differencing is used, as it requires two additional nodes in each horizontal direction for the difference operators.
In the solution first employed in the numerical experiments, two lines of auxiliary points were used, the values there being set in accordance with the boundary conditions. This procedure results in a loss of the fourth-order accuracy except at a truly symmetric boundary. To avoid this we later employed a method introduced by Oliger [11] utilizing third-order uncentered differences at the boundaries and retaining an overall fourth-order convergence.

6. Discussion of the Results

Two series of numerical experiments were conducted. One in November 1974 consisted of 24-hour forecasts using the three-parameter baroclinic model with second- and fourth-order differences for the 1000, 500 and 200 mb pressure surfaces. A dissipation factor using $\epsilon = 0.6$ in the x-direction only was included in the fourth-order model.
The second series of experiments was conducted for the winter period of February 1976 and was in all respects similar to the first series of experiments except that the dissipation factor used was $\epsilon = 0.015$ in the x and y directions in a variable relaxation factor was used for solving the Poisson eq. (1). The results were then compared with corresponding figures of the actual synoptic situation as obtained 24 hours later. The correlation coefficient between the forecast and the actual contour heights as well as the root mean square error (RMSE) were calculated for 24-hour forecasts of the same synoptic hour at the 1000, 500 and 200 mb surfaces respectively.

6.1 A Synoptic Comparison Between, Second- and Fourth-Order Forecasts

We shall illustrate in detail a synoptic situation using 24-hour forecast of the 500 mb pressure surface maps obtained by the second- and fourth-order models respectively. This discussion will outline experimentally the improvement in the phase speed error due to use of the fourth-order accurate space differences.
Fig. 1 shows the initial contour analysis of the 500 mb pressure surface at 0000 GMT of 28 February 1976. On the eastern part of the map we observe

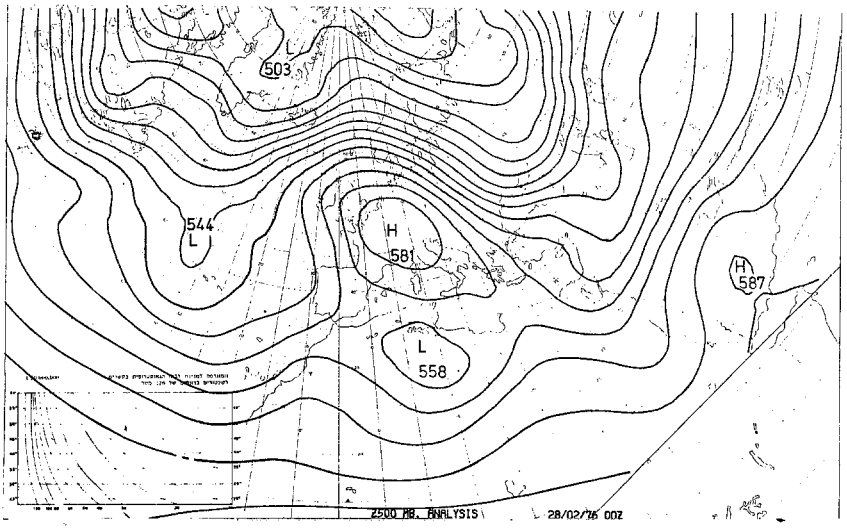

Fig. 1. Actual synoptic 500 mb height field analysis at 0000 GMT of 28 February 1976

a trough which has crossed the shores of Israel; beyond it, over the Black Sea, a small ridge is penetrating. A secondary trough is developing in the south-western part of the Black Sea.

The second-order 24-hour forecast (Fig. 2) for the 500 mb surface good for 0000 GMT of 29 February 1976 shows the secondary trough that was previously over the Black Sea to have penetrated to the south – up to the south-western part of Turkey. The small ridge has passed over Israel.

The corresponding fourth-order 24-hour forecast (Fig. 3) has the same essential features, with the following differences. The trough has penetrated more deeply and the trough-line is displaced by 2° to the East. The ridge, which is very weak, is also found to be further east.

The actual situation, viz. the 500 mb contour analysis at 0000 GMT of 29 February 1976 (Fig. 4) is better approximated by the fourth-order 24-hour forecast (Fig. 3). The ridge has almost disappeared and the trough has widened, its western part being along the line joining the centre of Turkey to the south-west of Cyprus.

The penetration of the trough towards the south more closely resembles in its extent the fourth-order forecast than that of second order. The evident shortcoming of the fourth-order 24-hour forecast as compared with the operative second-order one is the lower values it forecasts at the centres of high and low pressure. For instance, the high centre over Northern Italy has the values 5760 m for the second-order forecast (Fig. 2) and 5720 m for the

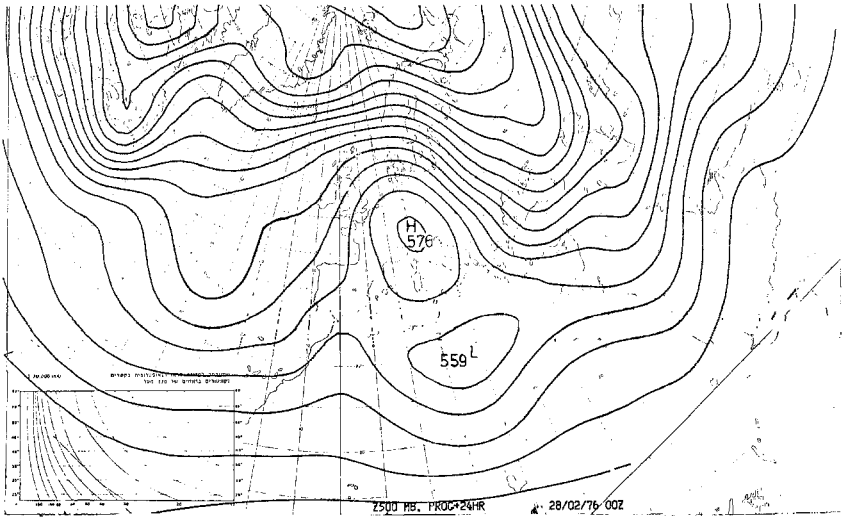

Fig. 2. Height field at 500 mb on 29 February 1976 (0000 GMT) using the operative second-order forecast model

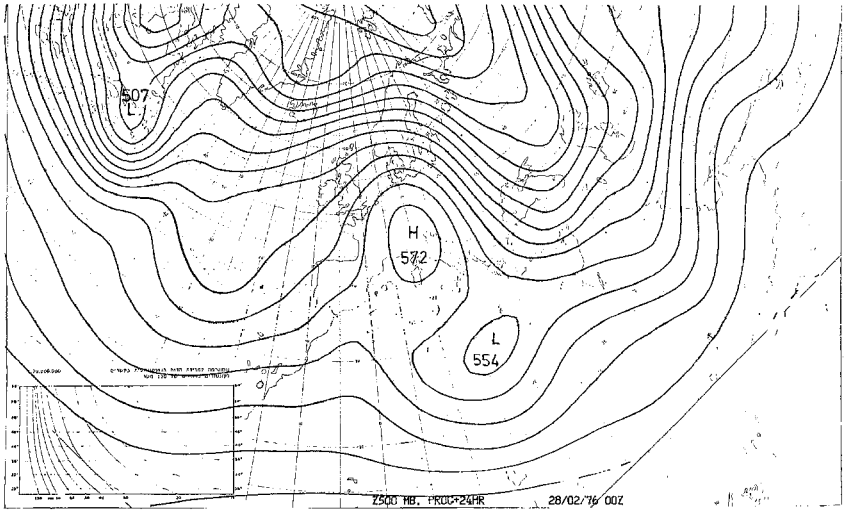

Fig. 3. Height field at 500 mb on 29 February 1976 (0000 GMT) using the fourth-order forecast model

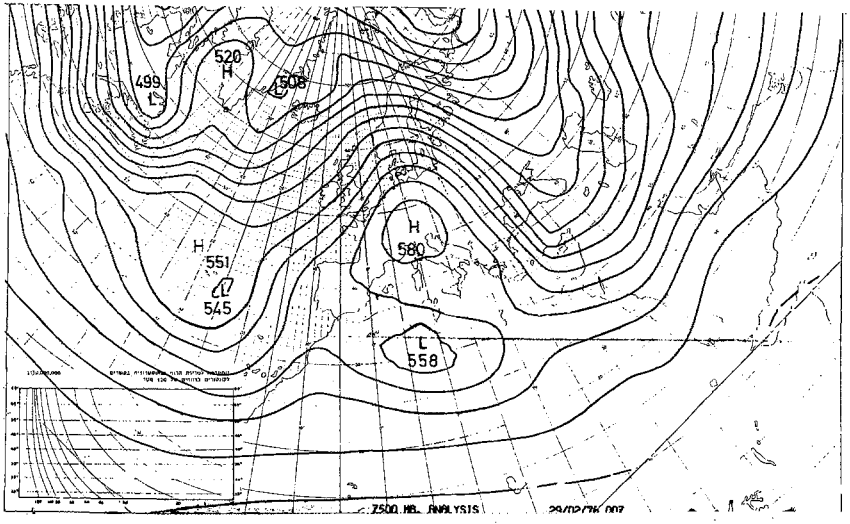

Fig. 4. Actual synoptic 500 mb height field analysis on 29 February 1976 (0000 GMT)

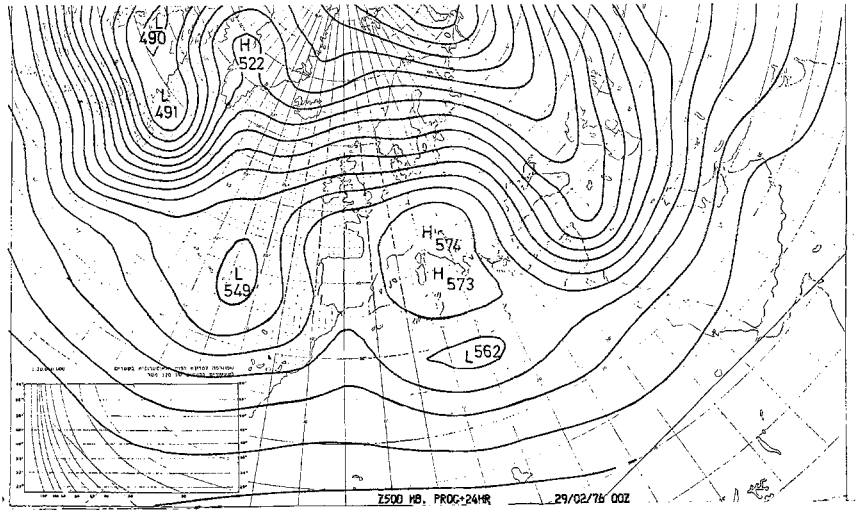

Fig. 5. Height field at 500 mb on 1 March 1976 (0000 GMT) using the operative second-order forecast model

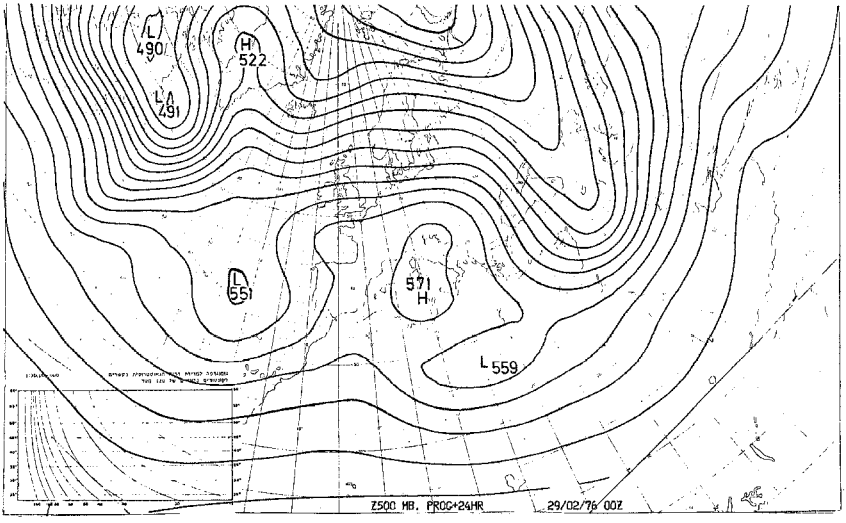

Fig. 6. Height field at 500 mb on 1 March 1976 (0000 GMT) using the fourth-order forecast model

fourth-order forecast (Fig. 3), while in the actual synoptic map the height is 5800 m (Fig. 4).

The low in North-Africa is 5590 m for the second-order forecast (Fig. 2); it is 5540 m for the fourth-order forecast (Fig. 3) and in the actual synoptic map it has a value of 5580 m (Fig. 4).

A very fast change occurred during the 24 hours following 0000 GMT of 29 February 1976 (see contour analysis map for 0000 GMT, 1 March 1976, Fig. 7). For instance, the trough line that was located west of Cyprus was shifted to longitude 40°E at 32° latitude, and at southern latitudes, to longitude lines 37°E–39°E.

The location of the trough in the 24-hour forecast map by the fourth-order model (Fig. 6) is nearer to the synoptic situation prevailing at 0000 GMT, 1 March 1976, than the 24-hour forecast map by the operative second-order model (Fig. 5).

In the second-order forecast the trough location is parallel to longitude lines 35°E–39°E, whereas in the fourth-order forecast it is parallel to longitude lines 37°E–40°E. But, again, the tendency is evident for the fourth-order forecast to give somewhat lower values at the pressure centres.

6.2 Verification Statistics for the Second- and Fourth-Order Forecasts

A verification program was run to compute statistical measures of the agreement between actual synoptic data and the forecast maps of the fourth-order

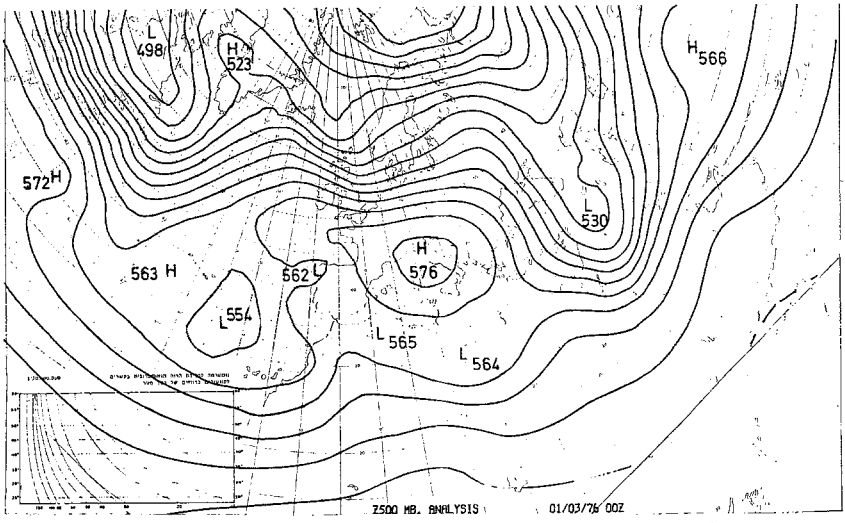

Fig. 7. Actual synoptic 500 mb height field analysis on 1 March 1976 (0000 GMT)

Table 1. *Statistics for 24-Hour Forecasts for November 1974.* (The verification relates to small control areas: Europe, the Mediterranean and North Africa.) ** fourth-order model + dissipation of $\epsilon = 0.6$ in the x direction only; * second-order operative model

Date	1000 mb				500 mb				200 mb			
	Corr		RMSE		Corr		RMSE		Corr		RMSE	
	**	*	**	*	**	*	**	*	**	*	**	*
1.11.74 00Z	.90	.82	26	29	.91	.82	38	50	.84	.65	39	52
3.11.74 00Z	.55	.63	31	19	.47	.50	44	37	.57	.60	56	56
5.11.74 00Z	.57	.63	66	44	.50	.55	55	45	.39	.22	71	68
9.11.74 00Z	–	.73	–	45	--	.72	–	46	–	.79	–	78
11.11.74 00Z	.75	.74	66	42	.76	.68	48	35	.85	.77	57	52
13.11.74 00Z	.88	.81	33	25	.83	.79	30	34	.83	.78	57	63
15.11.74 00Z	.42	.45	33	22	.72	.67	30	29	.77	.78	49	49
17.11.74 00Z	.66	.67	37	26	.40	.43	42	40	.26	.33	67	60
19.11.74 00Z	.77	.79	25	17	.87	.81	24	32	.87	.82	35	47
21.11.74 00Z	.76	.77	47	21	.68	.68	39	29	.80	.81	57	37
23.11.74 00Z	.79	.79	42	23	.87	.80	39	38	.90	.77	47	51
25.11.74 00Z	.80	.88	67	36	.84	.86	61	40	.72	.64	70	65

Table 2. *Statistics for 24-Hour Forecasts for February 1976*. ** fourth-order model + dissipation of $\epsilon = 0.015$ and variable relaxation factor in Poisson equation; * second-order model; L the entire forecast domain, S small control area (Europe, the Mediterranean and North Africa)

Date	1000 mb				500 mb				200 mb			
	Corr		RMSE		Corr		RMSE		Corr		RMSE	
	**	*	**	*	**	*	**	*	**	*	**	*
3.2.76 00Z	.53	.49	48	47	.71	.59	60	67	.47	.39	94	93 L
	.73	.63	31	32	.81	.74	53	51	.79	.76	82	64 S
8.2.76 00Z	.69	.63	38	39	.66	.64	55	52	.56	.52	87	82 L
	.66	.75	55	46	.55	.57	56	43	.44	.48	87	81 S
13.2.76 00Z	.72	.65	37	38	.68	.67	50	46	.58	.61	81	71 L
	.92	.89	23	23	.85	.81	35	40	.52	.42	56	59 S
15.2.76 00Z	.69	.61	45	42	.53	.51	54	51	.35	.32	85	83 L
	.37	.42	41	40	.44	.46	54	53	.68	.73	49	45 S
16.2.76 00Z	.60	.65	48	39	.68	.69	52	49	.55	.55	72	67 L
	.14	.26	44	27	.68	.73	53	42	.75	.79	63	49 S
20.1.76 00Z	.74	.73	34	32	.60	.54	56	56	.64	.58	73	74 L
	.73	.74	26	16	.68	.60	29	28	.55	.51	41	42 S
25.2.76 00Z	.81	.82	57	42	.67	.66	77	63	.45	.44	102	89 L
	.83	.89	80	32	.71	.62	104	68	.58	.61	145	104 S
27.2.76 00Z	.44	.42	69	49	.55	.55	72	55	.66	.64	70	66 L
	.55	.48	90	46	.83	.80	106	58	.75	.70	121	87 S
28.2.76 00Z	.55	.60	47	37	.53	.59	57	44	.62	.65	67	56 L
	.61	.66	64	33	.68	.72	81	51	.63	.74	91	57 S
29.2.76 00Z	.61	.58	43	39	.70	.67	48	48	.47	.40	71	70 L
	.70	.79	52	27	.83	.87	54	39	.69	.67	83	64 S

model (including the dissipative factor) and the second-order operative model (Tables 1 and 2). Mean statistics (correlation coefficient and RMSE) for the 24-hour 100, 500 and 200 mb forecasts using the fourth- and second-order models were computed.

The results show that the fourth-order scheme is superior to that of second-order when correlation coefficients are compared for the 200 and 500 mb levels, while no definite conclusion can be drawn for the 1000 mb level. However, the RMSE of the fourth-order scheme is greater than that of the second-order scheme whereas a decrease could have been expected [7]. The introduction of the dissipation factor may account for this result.

As the fourth-order scheme gave us a better estimate of the change in position and intensity of the synoptic system, specific statistics may be required to account for the improved location of the pressure centres due to the use of the fourth-order scheme.

7. Conclusions

The results obtained using fourth-order horizontal finite differences in the three-parameter baroclinic quasigeostrophic model are quite encouraging. A better location of the high- and low-pressure centres was obtained, indicating a significant reduction of the phase error.
As, however, other errors such as vertical truncation errors are associated with the use of the operative numerical forecasts, and as simplified physics is used in the construction of the model, the improvement due to the use of the fourth-order scheme is limited. It appears that the improvement is more limited on sea or desert regions where there are fewer reporting stations.
The lowering of the values at the pressure centres by the fourth-order scheme remains to be explained.
It is felt by the authors that the use of a compact fourth-order scheme suggested recently by Kreiss [13], which is effectively a three-point scheme, would further reduce the truncation error (see [5] and [6]) and that this scheme would have the further advantage that boundary conditions should be easier to impose.

Appendix

The detailed expressions for the symbols E, F, G, L, M, N are given below.

$$E = \frac{2f(D-C)\left(2\left(\nabla^2\psi + \frac{f}{\beta^2}\right) - \frac{g}{f}\nabla^2 h_0'\right)}{g(p_0-p_1)(AD-BC)}$$

$$F = \frac{2f(A-B)\left(2\left(\nabla^2\psi + \frac{f}{\beta^2}\right) - \frac{g}{f}\nabla^2 h_0'\right)}{g(p_0-p_1)(AD-BC)}$$

$$G = \frac{2f\beta^2\left(2\left(\nabla^2\psi + \frac{f}{\beta^2}\right) - \frac{g}{f}\nabla^2 h_0'\right)\left(\frac{H(D-C)}{\beta^2} + \frac{I(A-B)}{\beta^2}\right)+}{g(p_0-p_1)(AD-BC)}$$

$$+ \frac{f}{g}J\left(\psi, \frac{\beta^2 g}{f}\nabla^2 h_0'\right) + J\left(h_0', \beta^2\nabla^2\psi + f - \frac{\beta^2 g}{f}\nabla^2 h_0'\right)$$

$$L = \frac{2f(D+C)\left(2\left(\nabla^2\psi + \frac{f}{\beta^2}\right) + \frac{g}{f}\nabla^2 h_1'\right)}{g(p_0 - p_1)(AD - BC)}$$

$$M = \frac{-2f(A+B)\left(2\left(\nabla^2\psi + \frac{f}{\beta^2}\right) + \frac{g}{f}\nabla^2 h_1'\right)}{g(p_0 - p_1)(AD - BC)}$$

$$N = \frac{2f\beta^2\left(2\left(\nabla^2\psi + \frac{f}{\beta^2}\right) + \frac{g}{f}\nabla^2 h_1'\right)\left(\frac{H(D+B)}{\beta^2} - \frac{I(A+B)}{\beta^2}\right)}{g(p_0 - p_1)(AD - BC)} +$$

$$\frac{f}{g} J\left(\psi \frac{\beta^2 g}{f}\nabla^2 h_1'\right) + J\left(h_1', \beta^2\nabla^2\psi + f + \frac{\beta^2 g}{f}\nabla^2 h_1'\right).$$

A, B, C, D, E' and F' are respectively:

$$A = \frac{R\Gamma_0}{2g}\left[\frac{8p_0p_1}{(p_0 - p_1)^2}\log_e\left(\frac{p_0 + p_1}{2p_0}\right) + \frac{p_0 + 3p_1}{(p_0 - p_1)}\right]$$

$$B = \frac{R\Gamma_0}{2g}\left[\frac{4p_0(p_0 + p_1)}{(p_0 - p_1)^2}\log_e\left(\frac{p_0 + p_1}{2p_0}\right) + \frac{(3p_0 + p_1)}{(p_0 - p_1)}\right]$$

$$C = \frac{R\Gamma_1}{2g}\left[\frac{8p_0p_1}{(p_0 - p_1)^2}\log_e\left(\frac{2p_1}{p_0 + p_1}\right) + \frac{3p_0 + p_1}{(p_0 - p_1)}\right]$$

$$D = \frac{R\Gamma_1}{2g}\left[\frac{-4p_1(p_0 + p_1)}{(p_0 - p_1)^2}\log_e\left(\frac{2p_1}{p_0 + p_1}\right) - \frac{(p_0 + 3p_1)}{(p_0 - p_1)}\right]$$

$$E' = \frac{R\Gamma_0}{g}\left[\frac{7p_1 - 3p_0}{8(p_0 - p_1)} + \frac{p_1^2}{(p_0 - p_1)^2}\log_e\left(\frac{p_0 + p_1}{2p_0}\right)\right]$$

$$F' = \frac{R\Gamma_1}{g}\left[\frac{5p_1 - p_0}{8(p_0 - p_1)} - \frac{p_1^2}{(p_0 - p_1)^2}\log_e\left(\frac{p_0 + p_1}{2p_1}\right)\right]$$

Acknowledgements

Thanks are extended to the Numerical Weather Prediction and Computer Group at the Israeli Meteorological Service for their general support and in particular for making available meteorological data. The authors are indebted to Mrs. Tamar Ben-Amram for her many useful comments.

References

1. Arakawa, A.: Computational Design for Long Term Numerical Integration of the Equations of Fluid Motion: Two Dimensional Incompressible Flow. Part 1. J. Comp. Physics, *1*, 119–143 (1966).
2. Bushby, F. H., and C. J. Whitelam: A Three Parameter Model of the Atmosphere Suitable for Numeric Integration. Quart. J. Roy. Meteor. Soc., *87*, 374–392 (1961).
3. Gerrity, J. P., Jr., R. D. McPherson, and R. D. Polger: On the Efficient Reduction of Truncation Error in Numerical Weather Prediction Models. Mon. Wea. Rev., *100*, 637–643 (1972).
4. Grammeltvedt, A.: A Survey of Finite Difference Schemes for the Primitive Equations for a Barotropic Fluid. Mon. Wea. Rev., *97*, 384–405 (1969).
5. Hirsch, R. S.: Application of a Fourth-Order Differencing Technique to Fluid Dynamics Problems. Paper presented at SIAM 1974 Fall Meeting, 1974, Alexandria V. A.
6. Hirsch, R. S.: Higher-Order Accurate Difference Solutions of Fluid Mechanics Problems by a Compact Differencing Technique. J. Comp. Physics, *19*, 90–109 (1975).
7. Kálnay-Rivas, E.: Numerical Experiments With Fourth-Order Conservative Finite Differences. G.I.S.S. report. (In preparation.)
8. Kreiss, H. O., and J. Oliger: Comparison of Accurate Methods for the Integration of Hyperbolic Equations. Tellus, *24*, 199–215 (1972).
9. Kreiss, H. O., and J. Oliger: Methods for the Approximate Solution of Time Dependent Problems. GARP Publ. no. 10 (1973).
10. Kurihara, Y.: On the Use of Implicit and Iterative Methods for the Time Integration of the Wave Equation, Mon. Wea. Rev., *93*, 33–46 (1965).
11. Oliger, J.: Fourth-Order Difference Methods for the Initial Boundary Value Problem for Hypberbolic Equations. Maths. of Comp., *38*, 15–25 (1974).
12. Orszag, S. A.: Numerical Simulation of Incompressible Fluids Within Simple Boundaries: Accuracy. J. Fluid Mech., *49*, 75–112 (1971).
13. Orszag, S. A., and M. Israeli: Numerical Simulation of Viscous Incompressible Flow. Ann. Rev. Fluid Dyn., 281–318 (1974).
14. Roberts, K. V., and N. O. Weiss: Convective Difference Schemes. Maths. Comp., *20*, 272–299 (1966).
15. Sundström, A.: A Truncation Error Reducing Scheme for Balanced Forecast Models. Mon. Wea. Rev., *97*, 150–154 (1969).
16. Williamson, D. L., and G. L. Browning: Comparison of Grids and Difference Approximations for Numerical Weather Prediction Over a Sphere. J. App. Meteor., *12*, 264–274 (1973).
17. Thompson, P. D.: Numerical Weather Analysis and Prediction. New York: Macmillan Company. 1971.

Authors' addresses: I. M. Navon, National Research Institute for Mathematical Sciences, CSIR, P. O. Box 395, Pretoria 0001, South Africa; Z. Alperson, The Israeli Meteorological Service, P. O. Box 25, Beth-Dagan, Israel.